Lift/Drag Prediction of 3-Dimensional WIG Moving Above Free Surface

Seung-Hyun Kwag*

School of Mechanical Engineering, Halla University

The aerodynamic effects of a 3-dimensional Wing in Ground Effect (WIG) which moves above the free surface has been numerically investigated via finite difference techniques. The air flow field around a WIG is analyzed by a Marker & Cell (MAC) based method, and the interactions between WIG and the free surface are studied by the pressure distributions on the free surface. Waves are generated by the surface pressure distribution, and a Navier-Stokes solver has been employed, to include the nonlinearities in the free surface conditions. The pressure values Cp and lift/drag ratio are reviewed by changing the height/chord ratio. In the present computations a NACA0012 airfoil with a span/chord ratio of 3.0 are treated. Through computational results, it is confirmed that the free surface can be treated as a rigid wavy wall.

Key Words : Free Surface, WIG (Wing in Ground) Effect, Navier-Stokes, NACA0012, Lift/ Drag Ratio, Hydrodynamic Effect, PAR (Power Augmented Ram)

1. Introduction

As a potential candidate for high speed transportation, the wing in ground effect (WIG) demonstrates features of both an airplane and a ship. It gives us a new concept of a highly efficient vessel operating at over 100 knots. A wing operating in close proximity to the ground exhibits a reduction in induced drag, which increases the lift/drag ratio. For several decades, this phenomenon has been investigated since it complicates the takeoff and the landing of an advancing wing craft near the ground (Lippisch; 1964, Lockeed, 1962). During the 1970's, small experimental WIG vehicles were designed and tested in a coastal sea environment. However, it was noticed that these vehicles had a high structural weight fraction and an undesirably high takeoff/cruise power ratio. In the mid to late 1970's, the power

---
* E-mail : shkwag@hit.halla.ac.kr
  TEL : +82-33-760-1233 ; FAX : +82-33-760-1138
  School of Mechanical Engineering, Halla University
  66 Heungup, Wonju, Kangwon-do 220-712, Korea.
  (Manuscript Received June 23, 2000; Revised December 5, 2000)

augmented ram (PAR) phenomena were discovered, and it significantly enhanced the performance of the WIG concept (Smithey, 1977). At low speeds, a static pressure rise occurs under the wings, which lifts the craft out of the water. The development of WIG/PARWIG crafts have been made mainly for military uses. The Russian technology for these crafts are the most advanced in the world. Recently, the interest in super-high speed ships is rapidly growing worldwide. Among several types of crafts along these lines, the PARWIG craft is a potential candidate for fast sea transport. These can be used as naval and passenger ships, cargo/container vessels, and marine leisure craft.

In previous investigations the free surface has often been replaced by a rigid wall in the potential flow model (e.g. Masuda, 1991). In the present study, the effect of the free surface is numerically investigated by solving the Navier-Stokes equation including the viscous terms. The pressure distributions and velocity vectors are simulated around the upper and lower surfaces of the wing. The variations in Cp and lift/drag ratio due to changing values of height/chord ratio and of angle of attack are analysed. Specifically, a

NACA 0012 airfoil with a span/chord ratio of 3. 0 is treated. The present results indicate that the influence of the free surface is not significant in generating waves.

2. Numerical Scheme

2.1 Governing equation

Numerical simulations of 3-D free-surface flows are carried out by using the Marker and Cell (MAC) method. The velocity components u, v and w at time step (n + 1) are determined by

$$u^{n+1} = (F^n - \Phi_x^n)\Delta t,$$
$$v^{n+1} = (G^n - \Phi_y^n)\Delta t, \qquad (1)$$
$$w^{n+1} = (H^n - \Phi_z^n)\Delta t$$

where

$$F^n = \frac{u^n}{\Delta t} + \left(\frac{1}{Re} + v_t\right)\nabla^2 u - \left(u^n\frac{\partial u}{\partial x} + v^n\frac{\partial u}{\partial y}\right.$$
$$+ w^n\frac{\partial u}{\partial z}\right) - \frac{\partial}{\partial x}\left\{v_t\left(2\frac{\partial u}{\partial x}\right)\right\}$$
$$- \frac{\partial}{\partial y}\left\{v_t\left(\frac{\partial u}{\partial y} + \frac{\partial v}{\partial x}\right)\right\} - \frac{\partial}{\partial z}\left\{v_t\left(\frac{\partial u}{\partial z}\right.\right.$$
$$\left.\left.+ \frac{\partial w}{\partial x}\right)\right\},$$
$$G^n = \frac{v^n}{\Delta t} + \left(\frac{1}{Re} + v_t\right)\nabla^2 v - \left(u^n\frac{\partial v}{\partial x} + v^n\frac{\partial v}{\partial y}\right.$$
$$+ w^n\frac{\partial v}{\partial z}\right) - \frac{\partial}{\partial x}\left\{v_t\left(\frac{\partial u}{\partial y} + \frac{\partial v}{\partial x}\right)\right\}$$
$$- \frac{\partial}{\partial y}\left\{v_t\left(2\frac{\partial v}{\partial y}\right)\right\} - \frac{\partial}{\partial z}\left\{v_t\left(\frac{\partial v}{\partial z} + \frac{\partial w}{\partial y}\right)\right\},$$
$$\qquad (2)$$
$$H^n = \frac{w^n}{\Delta t} + \left(\frac{1}{Re} + v_t\right)\nabla^2 w - \left(u^n\frac{\partial w}{\partial x} + v^n\frac{\partial w}{\partial y}\right.$$
$$+ w^n\frac{\partial w}{\partial z}\right) - \frac{\partial}{\partial x}\left\{v_t\left(\frac{\partial u}{\partial z} + \frac{\partial w}{\partial x}\right)\right\}$$
$$- \frac{\partial}{\partial y}\left\{v_t\left(\frac{\partial v}{\partial z} + \frac{\partial w}{\partial y}\right)\right\} - \frac{\partial}{\partial z}\left\{v_t\left(2\frac{\partial w}{\partial z}\right)\right\},$$

and

$$\Phi^n = p + \frac{z}{Fn^2} \qquad (3)$$

$$\nabla^2 = \frac{\partial}{\partial x^2} + \frac{\partial}{\partial y^2} + \frac{\partial}{\partial z^2} \qquad (4)$$

Differentiating Eq. (1) with respect to x, y and z results in the following equation.

$$\nabla^2\Phi = F_x + G_y + H_z - (u_x^{n+1} + v_y^{n+1}$$
$$+ w_z^{n+1})/\Delta t \qquad (5)$$

The last term in Eq. (5) is expected to be zero to satisfy the continuity condition. Equation (5) can be solved by a relaxation method. The new free-surface at the (n + 1)th time-step is calculated by moving the marker particles by

$$x^{n+1} = x^n + u^n\Delta t,$$
$$y^{n+1} = y^n + v^n\Delta t, \qquad (6)$$
$$z^{n+1} = z^n + w^n\Delta t$$

It is desirable to introduce coordinate transformations in order to simplify the computational domain.

$$\xi = \xi(x, y, z), \quad \eta = \eta(x, y, z) \text{ and}$$
$$\zeta = \zeta(x, y, z) \qquad (7)$$

Through transformations, Eq. (1) can be written,

$$q_t + Uq_\xi + Vq_\eta + Wq_\zeta = \left(\frac{1}{Re} + v_t\right)\Delta^2 q$$
$$- K - REYSF(\xi, \eta, \zeta) \qquad (8)$$

where U, V and W are the contravariant velocities and K is the pressure gradient. The free surface is updated by moving the marker particles by

$$\delta\zeta/\delta t + u \cdot \delta\zeta/\delta x + v \cdot \delta\zeta/\delta y - w = 0|_{z=\zeta} \qquad (9)$$

The pressure is calculated by the following Poisson equation,

$$\Phi^{m+1} = \Phi^m + \omega \cdot (\Phi^{m+1} - \Phi^m) \qquad (10)$$

where (m + 1) denotes the next time step and ω is a relaxation factor.

2.2 Computational procedure and boundary conditions

Navier-Stokes (N−S) and Poisson equations are solved after the transformation. The calculation proceeds through a sequence of loops which advance the entire flow configuration through sufficiently small finite time increment. The computation is performed until the state becomes steady. An Euler explicit scheme is used for the time marching procedure. Pressure is obtained throughout the fluid domain by solving the Poisson equation. Iterations are automatically stopped when the pressure difference between two consecutive approximations is smaller than a certain quantity ε, chosen a priori. The new pressure field generates a new velocity field. The

velocity component is updated by using the time-forward difference form of the momentum equations.

In the present computations, two regions air above the free surface and water below it, are numerically coupled to satisfy the kinematic and dynamic free surface boundary conditions. The upper and lower parts are calculated in turn by using the boundary values of the other part. The pressure and velocity on the free surface are adopted as the boundary value for the calculation of the other domain. The procedure is repeated until a steady solution is obtained. The marker particles are moved to their new positions by using either Lagrange or Euler techniques. The flow starts from rest and is accelerated up to a given constant velocity for numerical stability. A third order upstream difference is used for convection terms. For example ;

$$U \cdot (\delta f/\delta x)_{i,j,k} = U_{i,j,k} \cdot (f_{i-2,j,k} - 8f_{i-1,j,k} + 8f_{i+1,j,k} - f_{i+2,j,k})/12 + |U_{i,j,k}| \cdot (f_{i-2,j,k} - 4f_{i-1,j,k} + 6f_{i,j,k} - 4f_{i+1,j,k} + f_{i+2,j,k})/4 \qquad (11)$$

The boundary conditions for off-PAR are as follows. Upstream, the flow starts from zero and is accelerated up to the predefined speed. Thus, the horizontal component of velocity is constant at all times. The vertical component is equal to zero at the upstream boundary and remains the same during the pressure computation. Downstream, the wavy motion influence is so gentle that the zero gradient extrapolation is used for both components of velocity and pressure. On the body surface, the no-slip and Neumann condition are used for velocity and pressure, respectively. The details on the free-surface condition can be found in (Lungu, 1994).

3. Results and Discussion

3.1 Computational conditions

A NACA 0012 airfoil with a span/chord ratio of 3.0 is treated. The angles of attack are 4°, 6° and 10°. The height/chord ratios from the ground are 0.1, 0.3, 0.8 at the Froude number of 0.56, and 0.3 & 0.7 at the Froude number 2.29 or more. The computing domain is 3.5 times as large as the

chord length in the streamwise direction. All parameters are non-dimensionalized based on the chord length L and uniform velocity U_o. The minimum grid spacing in the z direction is 0.002. The oncoming flow has been accelerated during the first 500 steps. The time increment Δt is 0.0005. The relaxation factor is 0.8 for the Poisson equation. The maximum number of iterations per step is 10 to 50, depending the pressure difference between the present and the next calculation. The grid is made of H-H topology to easily treat the free surface between air and water. A large number of iterations are needed near the leading edge. Figure 1 shows the coordinate system. The uniform flow direction, the lateral direction, and the normal direction are denoted by x, y and z, respectively. The PAR is located upstream to give the thrust by artificial air flows. Figure 2 shows a sectional view of the grid. Grid points are clustered near the body surface, tip, and trailing edge. The number of grids points are $101 \times 32 \times 44$ for
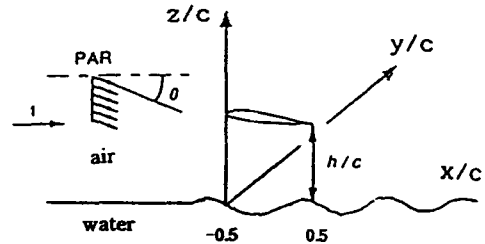

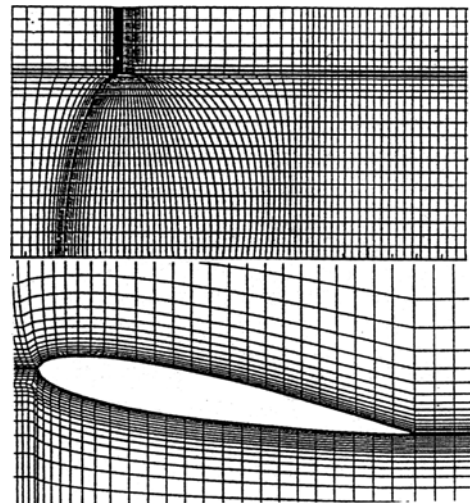**Fig. 1** Coordinate definition for computation

Fig. 2 Generation of 3-D computational grid

the air region and $101 \times 32 \times 10$ for the water region. The Reynolds number values of 10^3 10^6, 10^7, 10^8, 10^9 have been used for laminar and for turbulent flow calculations.

3.2 Computational results and discussions

Two kinds of computations are carried out to compare the effects of a free surface and those of a rigid wavy wall. Figure 3 is shows the rigid wall result for 4°, 6° and 10° angles of attack. The pressure contours are obtained at 4° and 6° angles of attack, and the velocity vectors are obtained at 10° angle of attack. The separation within the boundary layer is well captured. Since it is a

deeper case, there is no difference of flows between the two angles of attack. Table 1 compares predictions from the present method at 6° to present results a (Riegels, 1961; Abbott, 1958; Hirata, 1993). The lift prediction is reasonable. The total drag consists of pressure and frictional drag. For this laminar flow calculation, the frictional drag is greater.

Tables 2 and 3 lists the PAR effect at 10° angle of attack. According to the results, when the body approaches the ground, the velocity decreases below the wing due to the PAR effect, and the lift increases due to the pressure increase. In the simulation, the thrust is applied in the form of uniform flow for the PAR 1 and $-45°$ inclined flow for the PAR 2. The PAR is located one half chord length upstream of the leading edge as shown in Fig. 1. To investigate the PAR effect, the propulsor is artificially placed upstream of the wing, and the flow is accelerated through the wing at a 10° angle of attack. The thrust gives a 30% increase in the velocity by the momentum theory. Table 4 contains the effect of angle of attack, which shows a good trend in the lift. The
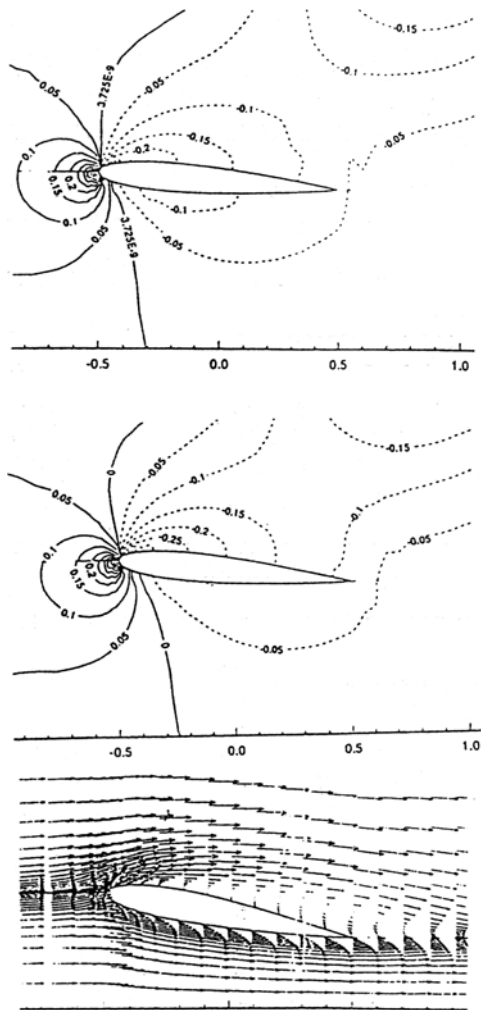

Fig. 3   Pressure and velocity at Fn=0.567 (off PAR, α=4°, 6°, 10° from above)

Table 1   Comparison of lift and drag coefficients

	Present solver	Hirata	BIEM	Abbott
C_L	0.6136	0.65	0.71	0.64
C_D	0.032	0.0117	—	0.0084

Table 2   Effect of PAR at h/c=0.10 and α=10°

	C_L	Cf	C_P	C_D	C_L/C_D
off PAR	1.0743	0.0106	0.081	0.092	11.7
PAR 1	1.2918	0.0109	0.082	0.093	13.9
PAR 2	1.4778	0.0113	0.082	0.093	15.9

Table 3   Effect of PAR at h/c=0.30 and α=10°

	C_L	Cf	C_P	C_D	C_L/C_D
off PAR	0.7875	0.0101	0.078	0.088	8.95
PAR 1	1.2262	0.0104	0.079	0.089	13.8
PAR 2	1.4523	0.0106	0.079	0.090	16.1

Table 4   Effect of angle-of-attack (α) at h/c=0.8

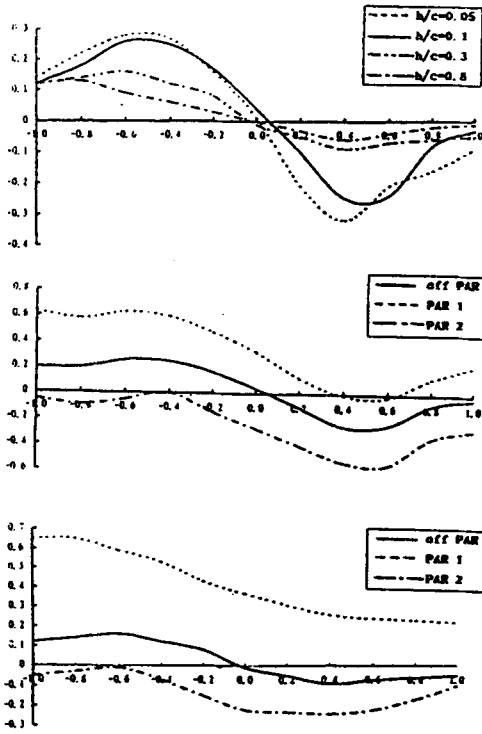|	C_L	Cf	C_P	C_D
$\alpha=10°$	0.7295	0.0101	0.074	0.084
$\alpha=6°$	0.6136	0.0099	0.032	0.042
$\alpha=4°$	0.5616	0.0104	0.028	0.038

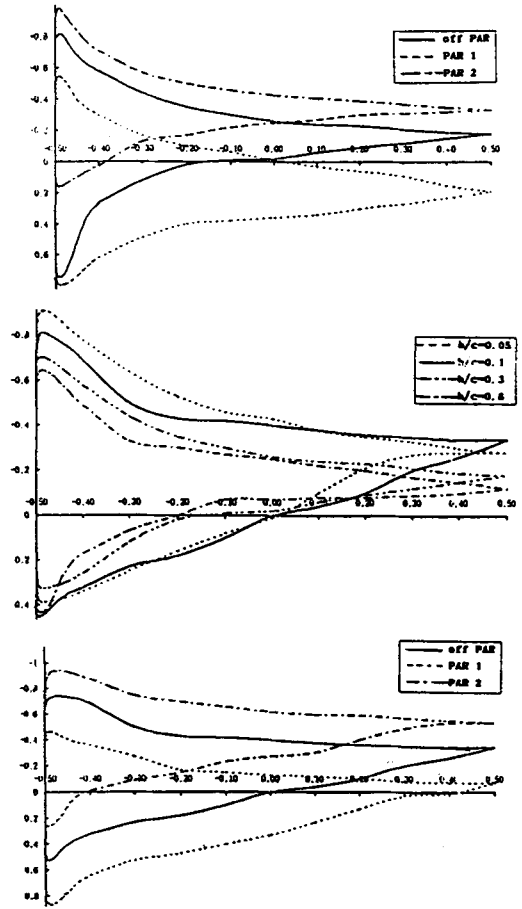

Fig. 4(a)   Pressure coeff. on ground surface

Fig. 4(b)   Pressure coeff. on wing surface

frictional drag is almost the same, while the pressure drag increases in proportion to the angle of attack.

Figure 4 shows the pressure coefficients due to ground effect. The PARWIG effect is large when the wing approaches the ground. Figure 4(a) indicates the pressure on the ground in which the first figure shows that the effect of height is very serious in the formation of pressure coefficients on the ground. The PAR effect can be seen in the two figures below. Figure 4(b) shows the pressure on the wing surface. The lift and drag can be calculated by integrating the pressure distribution. Figure 5 shows the results for the rigid wall case with a height/chord of 0.3, a Froude number
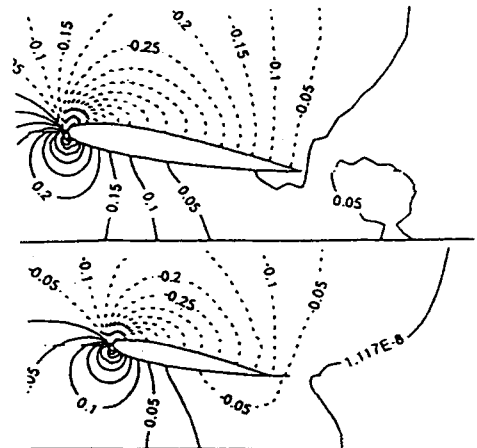

Fig. 5   Spanwise pressure at Fn=2.29 (wavy-wall cond. y/c=0.0, 1.0)

of 2.29, and a 10° angle of attack. Pressure distributions a at y/c=0.0 and y/c=1.0 are shown. The results show that 3-D flows can be well simulated in the spanwise direction. Figure 6 shows the results for the free surface case at the same conditions. The wriggle of pressure is seen under the leading edge and far behind the trailing-edge due to the existence of the free surface.
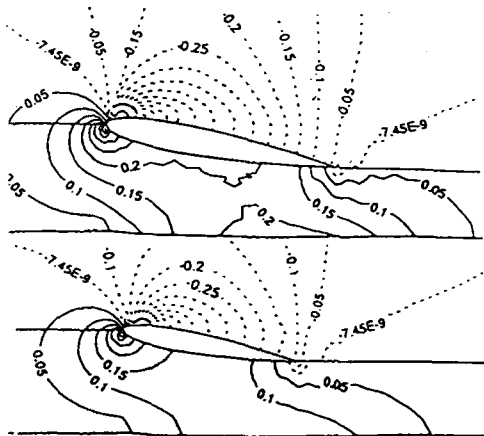
Figures 7 and 8 respectively show the rigid wall case results and the free-surface case results with a height/chord of 0.3, a Froude number of 4.58, and a 10° angle of attack. As seen, the pressure contour for these two cases are different. Thus, the pressure distribution and gradient are influenced by the free surface. The pressure gradient is stee-
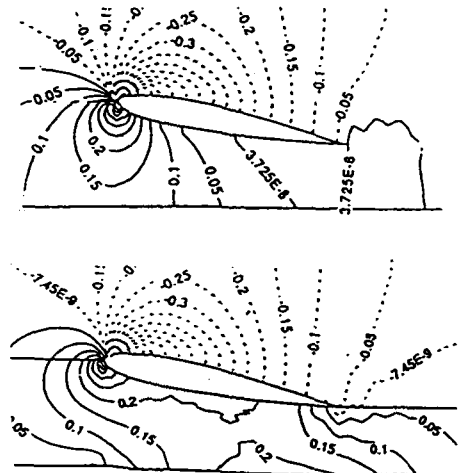

Fig. 6 Spanwise pressure at Fn=2.29 (free-surface cond. y/c=0.0, 1.0)

Fig. 8 Spanwise pressure at Fn=4.58, h/c=0.3 (above: w/o F.S., below: with F.S.)
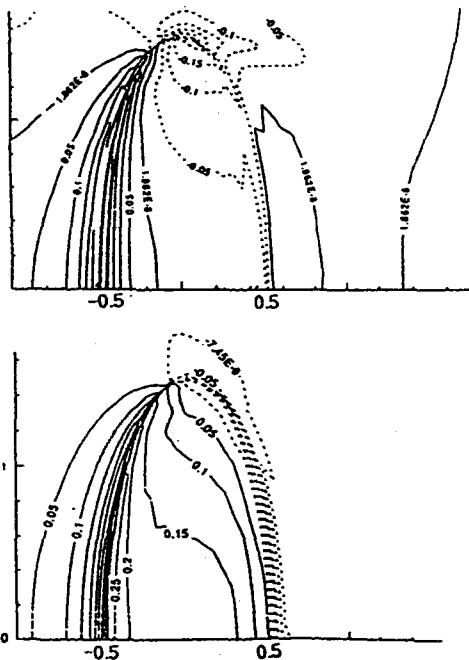

Fig. 7 Pressure contour on wing surface Fn=4.58, h/c=0.3 (above: w/o F.S., below: with F.S.)
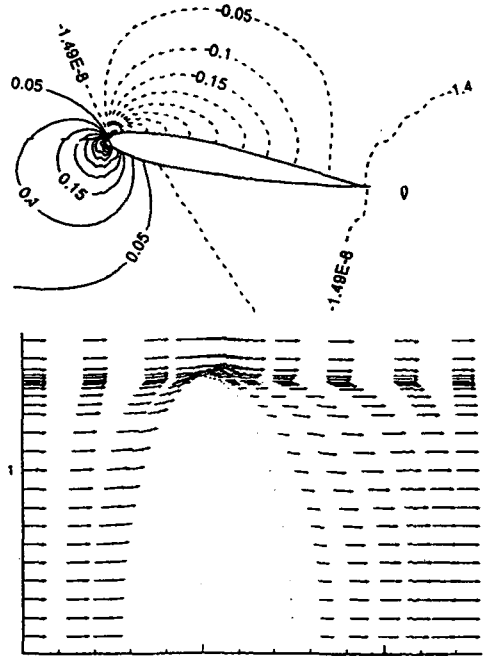

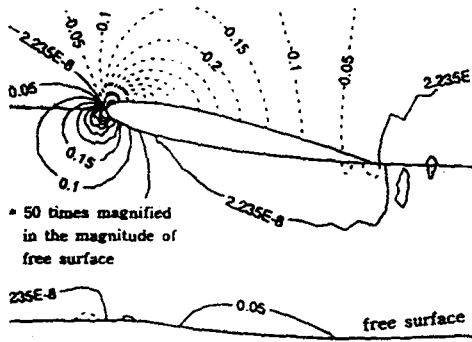**Fig. 9** Pressure and velocity vectors at Fn=2.29, h/c=0.7 without F.S.

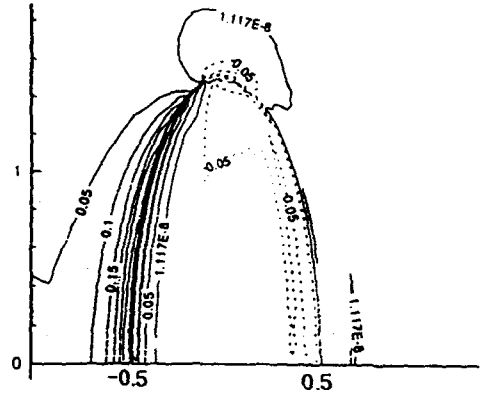Fig. 10   Pressure distribution at Fn=2.29, h/c=0.7 with F.S.

Fig. 11   Pressure distribution at Fn=3.5. h/c=0.1 with F.S. (a=3.5, 6, 8°)
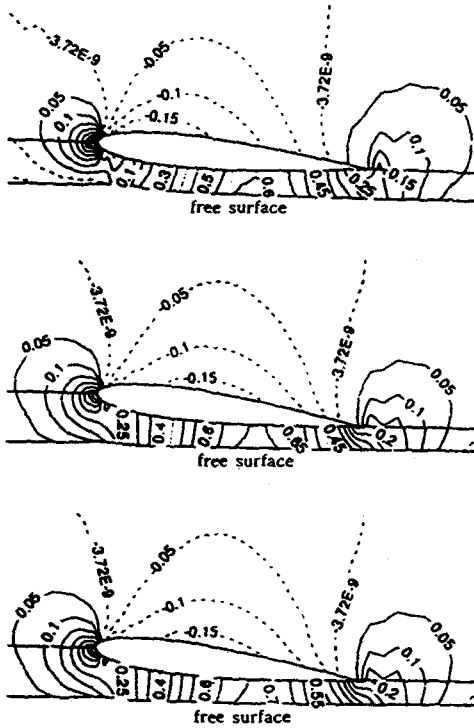

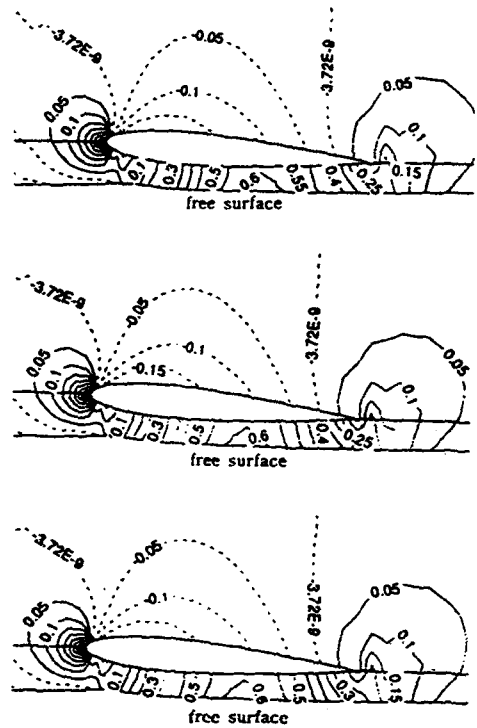Fig. 12   Pressure distribution at Fn=2.29, a=10°, Rn=10^6 with F.S.

Fig. 13   Pressure distribution at Fn=3.5. Rn=10^6, 10^8, 10^{10} from above, with F.S.

per behind the tip for the rigid surface case, while the ripple is visible in the free-surface case. Figures 9 and 10 show the results of rigid wall case and the free-surface case with a height/chord of 0.7, Froude number of 2.29, and a 10° angle of attack. It being a deeper case, the pressure gradient is less affected by the free surface. Thus, the height/chord ratio from the free surface is important to the pressure distribution and the develop-

ment of the free surface. Figure 11 shows the results when the body of the craft approaches the free surface. As the incidence angle increases, the wave behind the trailing-edge approaches the wing. In the lowest figure, the wave under the trailing-edge almost touches the wing. Even in this case, the computation was successfully made without any divergence. Figure 12 shows the
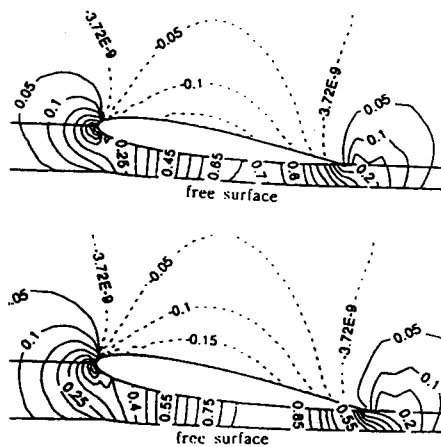
Fig. 14   Pressure distribution at Fn=3.5, Rn=10⁸, α=6. 8° from above, with F.S.

results with Reynolds numbe 10^6 and a $10°$ angle of attack. The pressure is retarded around the tip due to three dimensional effects. The pressure is well developed even at high Reynolds numbers. For the high Reynolds number flows, the Baldwin-Lomax turbulence model is used. Figure 13 shows the results for Reynolds numbers of 10^6, 10^8 and 10^{10} The Froude number is 3.5, and the angle of attach is 3.5°. From three cases above, the effects of Reynolds number can be confirmed. The pressure above the wing is practically the same. Below the wing, pressure is different due to the free surface. Figure 14 shows the effects of angle-of-attack at a Reynolds number of 10^8 with a free surface.

Conclusions

(1) Numerical simulations have been performed to clarify the 3-dimensional hydrodynamic effects of a WIG moving above the free surface. Waves are generated by the surface pressure distribution. A N-S solver was employed to capture the nonlinearities in the free surface conditions. For a detailed discussion of WIG and PARWIG, pressure values and lift/drag ratio are carefully reviewed by changing the height/chord.

(2) The flow field around a WIG is analyzed by a MAC-based method, and the interaction between the WIG and a free surface has been investigated. In the present computation, a

NACA 0012 airfoil with a span/chord ratio of 3. 0 is treated. The free surface effect is negligible in generating waves. But the pressure patterns are slightly different from the rigid wall case when the body approaches the free surface.

(3) A wing operating in close proximity to the ground exhibits a reduction in the induced drag and an increase in the lift/drag ratio. The lift is also influenced by a free surface, but the generated wave is not so large. The PAR phenomenon involves directing the efflux from forward mounted propulsion system with that nearly stagnated under the wing.

References

Abbott, I, H. and Von Doenhoff, A. E., 1958, "Theory of Wing Sections," Dover Publication, New York.

Hirata, N., 1993, "Simulation on Viscous Flow around Two Dimensional Power Augmented Ram Wing in Ground Effect," *Jour., Soc., Naval Arch. of Japan*, Vol. 174, pp. 47~54.

Lippisch, A. M., 1964, "The Aerodynamic Ground Effect and Development of the Aerofoil Boat," Luftfahrtechnik Raumfahrteknik 10, pp. 261~269.

Lockeed California Company Report, 1962, "Preliminary Economic Analysis of Winged Hull Vehicles," LA/ME/2148.

Lungu, A. and Mori, K., 1994, "Developments of the Finite Difference Schemes for Free-Surface Flow Computation," *Proc. Int. Workshop on CFD*, Tokyo, Vol. 1, pp. 331~340.

Masuda, K. and Suzuki, K., 1991, "Simulation of Hydrodynamic Effects of 2-Dimensional WIG Moving Near the Free Surface," *Jour. of Soc. of Naval Arch of Japan*, Vol. 170, pp. 83~92.

Riegels, F. W., 1961, "Aerofoil Sections," Butter worths, London.

Smithey, W. J. H., Papadales, B. S., Jr. and Chaplin, H. R., 1977, "Effect of Turbulent Jet Mixing on the Static Lift Performance of a Power Augmented Ram Wing," David Taylor Naval Ship Research and Development Centre ASED-389.